Proceeding of the IEEE
International Conference on Robotics and Biomimetics
Dali, China, December 2019

Prediction of TBM Tunneling Parameters through an LSTM Neural Network

Haowen Chen, Cai Xiao, Zhixiao Yao, Hao Jiang, Tao Zhang*, and Yisheng Guan

Biomimetic and Intelligent Robotics Lab (BIRL)
School of Electro-mechanical Engineering
Guangdong University of Technology
Guangzhou, Guangdong Province, China, 510006

***Abstract*—With the wide application of tunnel boring machines (TBMs) in tunnel construction, the adaptive tuning of the TBM tunneling parameters has become a research focus. Nowadays, since complicated geological conditions are still challenging to predict, the fine-tuning of tunneling parameters mainly relies on operational experience. Artificial intelligence provides a convenient solution for predicting tunneling parameters through data mining and machine learning. Based on *in-situ* data, this work proposed a novel method for segmenting the original data in tunneling cycles and analyzing the parameter correlation for data size reduction. Subsequently, a model was established based on an LSTM to predict tunneling parameters in the steady phase based on the data in the rising phase. The results demonstrated that the model is capable of predicting torque and thrust accurately. This makes it possible to adjust the TBM tunneling parameters according to current geological conditions in real time. The present study is of great significance for the tunneling efficiency and construction safety in the actual TBM construction, since it can improve its scientific and intelligent level.**

***Index Terms*—Tunnel Boring Machine; Parameter prediction; Long Short-Term Memory; Machine Learning**

I. Introduction

Tunnel boring machines (TBMs) are highly advanced equipment used in tunneling engineering. Due to their high efficiency, safety, and environmental friendliness, TBMs will become a trend in tunnel construction, replacing traditional drilling and blasting methods [1]. However, in traditional TBM operations, the operator needs to evaluate the rock conditions through a slow trial excavation phase, and then tune the tunneling parameters repeatedly until reaching a steady state. This process is dependent on operator experience, and leads to low construction efficiency. In addiction, when there is an extreme change in rock state, it is impossible to identify the surrounding rock conditions, which makes the tunneling parameters unable to adapt to the complicated and altered geological conditions. Such cases may easily cause serious engineering accidents and even casualties. Therefore, in order to ensure an efficient and safe construction, it is an urgent need to investigate methods of adjusting the TBM tunneling parameters adaptively based on the different geological conditions. Since it is still challenging to predict the geological conditions prior to excavation, an alternative method for improving the adjustability of TBM is the prediction of certain important tunneling parameters, such as the cutterhead thrust and torque, through *in-situ* data.

Currently, only a few studies have reported results on TBM tunneling parameters prediction [2, 3]. In particular, these studies have focused on the prediction of several TBM tunneling parameters [2]. In general, the prediction methods for TBM tunneling parameters can be classified into three categories: the empirical method [4, 5], the rock and soil mechanics method [6–8] and the numerical simulation method [9, 10].

In recent years, with the development of machine learning, researchers have begun to introduce machine learning into TBM tunneling parameters prediction. Tao et al. [11] and Sun et al. [12] used random forests to predict the penetrating rate and load parameters. Mahdevari et al. [13] applied the support vector regression to predict the penetrating rate. Ling et al. [14] combined the partial least squares regression algorithm with the fuzzy-neuron network to predict the penetrating rate. It is worth noting that several variants of the recurrent neural network (RNN) were applied by Gao et al. [15] to predict some parameters in real time. However, only short-term (in the next second) predictions of the parameters were made, rather than focusing on predicting the parameters in the steady phase. In engineering practice, the operator needs to estimate the control parameters of the steady phase in the rising phase. Therefore, the real engineering practice is limited to short-term predictions. The goal of the present study is to propose a method as a solution to this problem.

In this paper, 30 seconds data from the beginning of the rising phase were used to predict the tunneling parameters of the steady phase during TBM tunneling. In engineering practice, the predicted parameters can provide a reference for the TBM operators to estimate the forthcoming geological conditions and make appropriate decisions. Firstly, historical data were preprocessed and divided into many tunneling cycles, and each cycle was segmented into several phases. Then a method, called parameter identification, was proposed to identify the parameters that are critical to the tunneling parameters. After that, an LSTM-based network architecture was established, and it was trained and tested using the aforementioned data.

*Correspondending author, email: tzhang@gdut.edu.cn.

This work is financially supported by the Natural Science Foundation of China—Project for Young Scientist (Grant No. 51905105), and the Natural Science Foundation of Guangdong Province—Regular Project.

978-1-7281-6321-5/19//$31.00 ©2019 IEEE

II. LSTM Networks

The long short-term memory (LSTM) network, which was proposed in 1997 [16], is a special variant of RNN, where the connections between nodes form a directed graph along a temporal sequence. Any RNN and its variants have a trained form consisting of repetitive units, as shown in Fig. 1. In traditional RNNs, the repetitive unit alone has a very simple structure, such as a tanh layer. When dealing with long-term dependency problems, traditional RNNs involve multiple matrix multiplications, which lead to exploding and/or vanishing gradient problems. In order to solve such problems, many variants of RNN have been developed, such as the echo state network, the gated recurrent unit, and the LSTM. Among these variants, the LSTM is one of the most famous networks, which can solve the exploding and vanishing gradient problems.

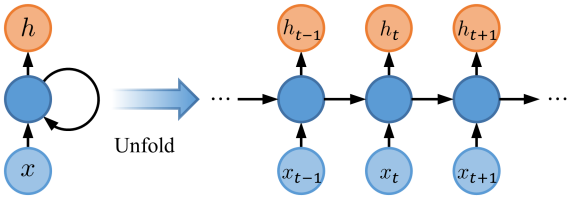

Fig. 1. Recurrent neural network and its unfolding form

As an RNN variant, LSTM has the same structure as RNN, i.e., it is connected by repetitive units. However, unlike the traditional RNN, the repetitive units of LSTM are composed of a cell state, an input gate, an output gate, and a forget gate (Fig. 2). The cell remembers values over arbitrary time intervals, while the three gates regulate the flow of information into and out of the cell. In Fig. 2, the blue circle represents the input of the network, the yellow boxes represent the learned neural network layers, and the orange shapes represent element-wise operations, such as element-wise addition.

The diagram in Fig. 2 is a typical LSTM unit. The key to LSTM is the cell state (C_t) that. When it runs straight down the entire chain, only some minor interactions occur. It is easy for the information to simply flow along the chain unaffected and maintain its integrity. The merging arrows represent vector concatenation, while the forking arrows represent vector duplication.

The gates in LSTM have been designed to remove or add information to the cell state. They are a composition of a sigmoid layer and multiplication operations. The sigmoid layer output is a value between 0 and 1, which indicates the weight of information flow. The LSTM achieves the control and protection of the cell state through these three gates.

The forget gate decides what information will be disposed of from the cell state. This transfer can be defined as:

$$f_t = \sigma\left(W_f \cdot [h_{t-1}, x_t] + b_f\right) \tag{1}$$

where σ is the sigmoid activation function, W_f is the weight of the connections between neurons, h_{t-1} is the output of the last neuron, x_t is the input of the current neuron, and b_f is

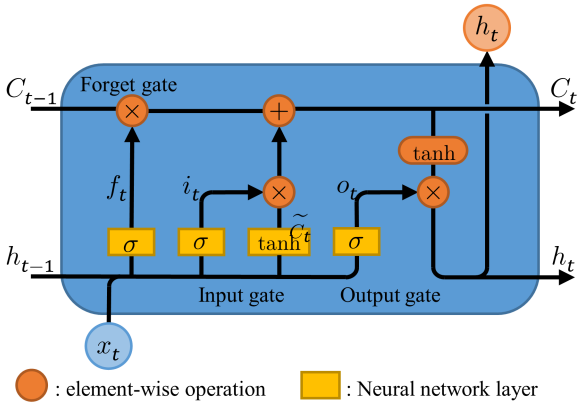

Fig. 2. LSTM cell diagram

the bias of neuron. The forget gate determines the effect of the input on the current cell state, and the preservation and discarding of the previous cell state.

The input gate determines how much new information will be stored in the current cell state. This transfer can be defined as:

$$i_t = \sigma\left(W_i \cdot [h_{t-1}, x_t] + b_i\right) \tag{2}$$

$$\tilde{C}_t = \tanh\left(W_C \cdot [h_{t-1}, x_t] + b_C\right) \tag{3}$$

where tanh is the activation function, and b_i and b_C are the biases of the neural network. The sigmoid layer decides which value will be updated, while the tanh layer creates a new vector $\tilde{C}$ which can be added to the cell state.

After completing the above steps, the updated cell state can be defined as:

$$C_t = f_t * C_{t-1} + i_t * \tilde{C}_t \tag{4}$$

where $*$ is an element-wise production operation. In the updating procedure of the cell state, the old cell state C_{t-1} is multiplied by f_t to forget some information, and then, the new candidate value $i_t * \tilde{C}_t$ from the input gate is added.

After the cell state has been updated, the output gate will output the current cell state. This transfer can be defined as:

$$o_t = \sigma\left(W_o \cdot [h_{h-1}, x_t] + b_o\right) \tag{5}$$

$$h_t = o_t * \tanh\left(C_t\right) \tag{6}$$

In summary, the above three gates are composed of sigmoid and tanh neural network layers, which help in the selection of effective information.

III. Parameter Prediction Modeling

A. Modeling Background

The data set used in the present study was *in-situ* data from the Water Supply Project of Jilin Province by Introducing Water from the Songhua River. The above project contains huge amounts of data collected from the TBM equipment, since a tunneling length of 17.488 km was constructed by TBM. During TBM tunneling, the TBM system recorded one group of data per second, containing 197 parameters.

In engineering practice, the TBM tunneling process consists of a series of tunneling cycles, each of which is about 1.8 m long. Each tunneling cycle can be divided into empty phase, a rising phase, and a steady phase. In the tunneling process, the TBM operator makes empirical assessments concerning the geological conditions based on the TBM tunneling parameters (e.g. thrust, torque, motor current, cutterhead power) variation during the rising phase, and then determines the TBM control parameters (e.g. rotational speed of cutterhead, advance velocity) to be set in the steady phase. The aim of TBM tunneling parameter prediction is to estimate some important TBM parameters in the steady phase through analyzing a sequence of data from the rising phase like an operator.

B. Modeling Method

The proposed workflow of the intelligent TBM tunneling process is demonstrated in Fig. 3. Initially, the historical data are preprocessed to obtain the valid part. Then, the LSTM network is trained, which will later use the data from the rising phase to predict the tunneling parameters in the steady phase. Concurrently, new data collected from the TBM are saved, and preprocessed to train the model and improve its accuracy.

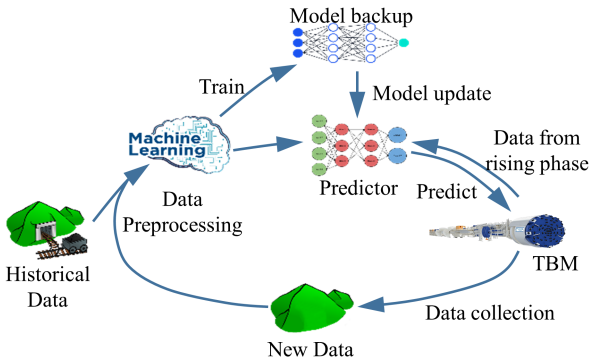

Fig. 3. Workflow of the intelligent TBM tunneling process

Firstly, data preprocessing is performed, where the first 30 seconds data during the rising phase are extracted from the original data set andany abnormal data are eliminated.

Then, the parameters that have a significant effect on thrust and torque in the steady phase are selected by parameter identification. Data correlation analysis combined with engineering experience is performed to reduce the data size. Benefiting from this, the network training time is reduced and the model accuracy is improved.

Finally, because the data from the rising phase are closely related to time, LSTM is chosen to make the prediction. The architecture of the neural network used in this study can be seen in Fig. 4. The input of the network is a sequence of 30 seconds data with n parameters from the rising phase. It should be mentioned that n depends on the parameter identification result. The output is the torque and thrust in the steady phase.

The ratio of the training set to the test set is 9:1. The model is validated using the test set, and its accuracy is evaluated using the mean absolute percentage error (MAPE) (7). In

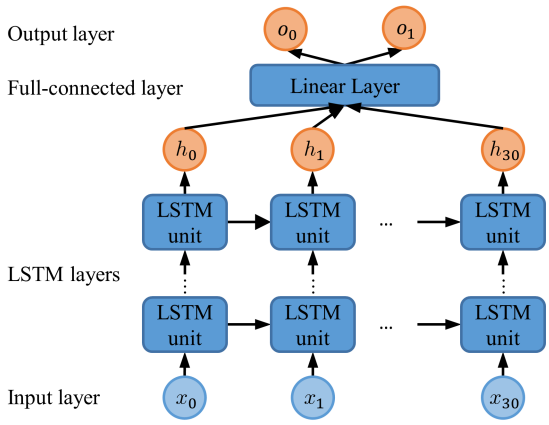

Fig. 4. Network architecture

order to achieve the highest precision possible, the model input dimension is optimized according to the evaluation results.

$$MAPE = \frac{1}{n}\sum_{i=1}^{n}\left|\frac{y-\hat{y}}{y}\right| \times 100\% \tag{7}$$

where n is the number of samples, y is the actual value, and $\hat{y}$ is the predicted value.

C. Data Preprocessing

The purpose of the data preprocessing step is to segment the tunneling cycles derived from the original data set, and then to divide each tunneling cycles into several phases. By analyzing the original data, it was found that the rotational speed of the cutterhead exhibited a significant cyclical change. Hence, the rotational speed was selected as the basis for segmenting the tunneling cycles. The transition between different phases in a tunneling cycle is closely related to the change in thrust. Therefore, the thrust was selected as the basis for segmenting the different phases.

The original data had 197 dimensions in one day, which can be given as:

$$\left\{x_i^{(j)}\right\}, (0{\le}i{\le}86400, 1{\le}j{\le}197) \tag{8}$$

where i is the time and j is the data dimension.

Let n be the rotational speed of the cutterhead, i.e., $n_i = x_i^{(121)}$, since the rotational speed was the 121-st dimension in the original data set. For the data from any day $\{x_i^{(j)}\}$, there exist $0{\le}k_1 < k_2{\le}86400$, which satisfy

$$n\begin{cases} {}_i{\neq}0, k_1{\le}i{\le}k_2 & (9) \\ k_2 - k1{\ge}300 & (10) \end{cases}$$

then $\{x_i^{(j)}|k_1{\le}i{\le}k_2\}$ is a tunneling cycle.

Let F be the thrust, k_0 be the start time of a cycle, k_1 be the start time of a rising phase, k_2 be the start time of a steady phase, k_3 be the end time of a steady phase, and k_4 be the end times of a cycle. Subsequently, the first- and second-order difference of the thrust F can be respectively presented as:

$$\Delta F_i = F_{i+1} - F_i \tag{11}$$

$$\Delta^2 F_i = \Delta F_{i+1} - \Delta F_i \tag{12}$$

The start and end times of the three phases in a tunneling cycle are determined by ΔF and $\Delta^2 F$. The start time of the rising phase k_1 can be defined as:

$$k_1 = \operatorname{argmax}\left(\Delta^2 F_i\right), k_0 < i < \operatorname{argmax}\left(\Delta F_i\right) \tag{13}$$

The start time of the steady phase k_2 can be defined as :

$$k_2 = \frac{\sum_{i=s}^{s+N} \Delta F_i}{N}, k_1 \leq s \leq k_3 \tag{14}$$

The end time of the steady phase k_3 can be defined as:

$$k_3 = \operatorname{argmin}\left(\Delta F_i\right) \tag{15}$$

where argmin and argmax are the points where the function value is minimized and maximized, respectively. Fig. 5 shows the data preprocessing results for one tunneling cycle.

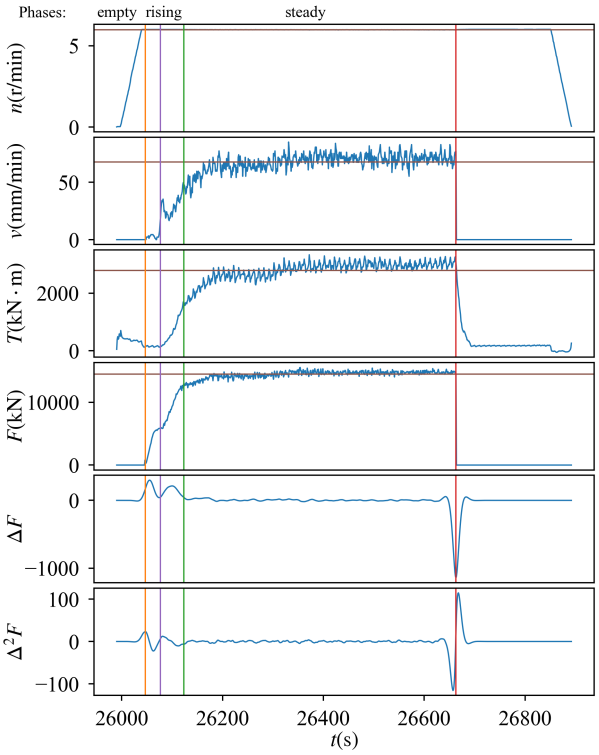

Fig. 5. Empty, rising and steady phases in a tunneling cycle.

D. Parameter Identification

From all the parameters, parameter identification selects the parameters that are critical to the model output and removes parameters that are irrelevant to the results. The correlation between load parameters (thrust and torque) and other parameters can be calculated using the Pearson correlation coefficient through the following steps:

1) Calculate the expected value:

$$\mathrm{E}[X] = \sum_{i=1}^{k} x_i p_i \tag{16}$$

where X is a random variable with a finite number of outcomes $x_1, x_2, \ldots, x_k$ which occur with probabilities $p_1, p_2, \ldots, p_k$, respectively.

2) Calculate the standard deviation:

$$\sigma = \sqrt{\mathrm{E}\left[(X-\mu)^2\right]} \tag{17}$$

where μ is the mean value of X, i.e., $\mu = \mathrm{E}(X)$

3) Calculate the covariance:

$$\operatorname{cov}(X,Y) = \mathrm{E}\left[(X - \mathrm{E}[X])(Y - \mathrm{E}[Y])\right] \tag{18}$$

4) Calculate the Pearson correlation coefficient:

$$\rho_{X,Y} = \frac{\operatorname{cov}(X,Y)}{\sigma_X \sigma_Y} \tag{19}$$

The data of each tunneling cycle had a total of 197 parameters, two of which were output parameters. After importing the data from 100 cycles, and calculating the Pearson correlation coefficient between the two output parameters and the remaining 195 parameters, the frequency of the parameters whose correlation coefficient exceeded 0.9 was counted.

The above frequency was used to sort the parameters, in order to determine an optimal number of input parameters. The 5, 10, 20, 30, 40, 80, 120, and 160 parameters with the highest frequency, all parameters, and the 42 parameters selected manually based on engineering experience, were selected as model inputs. The model was trained and tested using the aforementioned 10 test groups, each of which contained data from the same 1000 cycles. Then, the accuracy of each group was calculate by MAPE. The results are shown in Fig. 6.

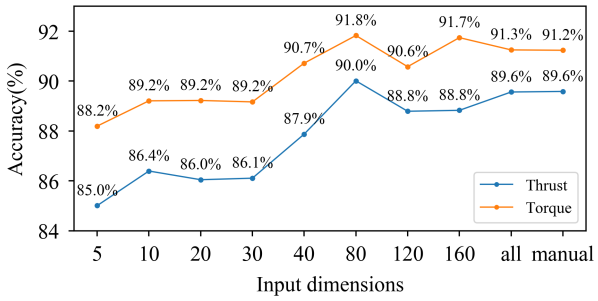

Fig. 6. Results of parameter identification

IV. Experiment

As it can be seen in Fig. 6, when the input was 80 parameters (the exact parameters are given in the Appendix), the model accuracy was the highest. In order to verify the accuracy of the model, these 80 parameters were used as model inputs to predict the thrust and torque in the steady phase. All tunneling cycles (4153 cycles in total) extracted from the original data set were divided into a training set and a test set by a ratio of 9:1. The model was trained and tested using the above data, and the test results are presented in Figs. 7 and 8.

The MAPE was used to evaluate the error of the test results. The errors of torque and thrust reached 10.48% and 8.82%, respectively.

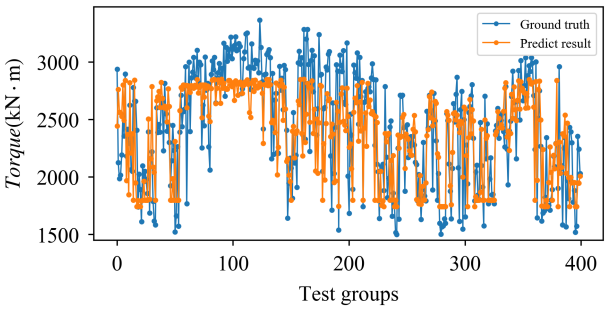

Fig. 7. Torque prediction results in the steady phase

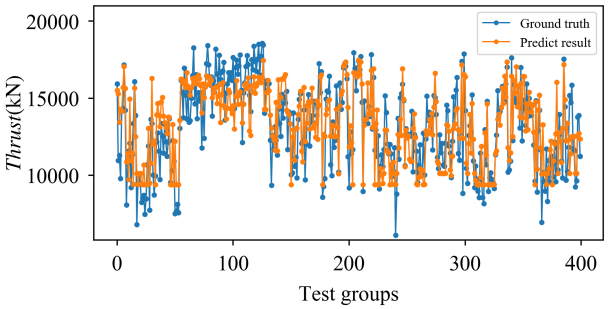

Fig. 8. Thrust prediction results in the steady phase

V. Conclusion

The original data set was initially preprocessed to extract the tunneling cycles, each of which was then segmented into several phases. Parameter identification was used to find the parameters with the greatest impact on the tunneling parameters. Then, due to its advantages in handling temporal sequence problems, LSTM was chosen to predict the tunneling parameters in the steady phase. Finally, the model was trained and tested, using the 80 optimal parameters as input. Based on the test results, the following conclusions can be drawn:

1) The proposed model established based on the LSTM neural network can effectively accomplish the mapping between parameters in the rising phase and the steady phase. The prediction accuracy of the model for torque and thrust was 89.52% and 91.18%, respectively, which provides a reliable reference for the operator to evaluate the geological conditions during operation. In addition, it provides the basis for the intelligent control of TBM, so that the TBM control parameters can be adjusted to the current geological conditions in real time.
2) Parameter identification is used to identify the parameters which have a significant impact on the tunneling parameters. This can reduce the size of the model input, significantly reducing the training time, while improving the accuracy of the model. In engineering applications, the above results show that it is possible to collect data of key parameters only, which can reduce the number of sensors, and thereby reduce the equipment costs.

This paper attempts to use the neural network to predict the TBM tunneling parameters, but there is still a certain distance from the actual engineering application. In the future, researchers can also explore the real-time perception of geological conditions, feedback control of tunneling process, and early warning of unfavorable geological conditions.

Acknowledgments

This work is financially supported by the Natural Science Foundation of China—Project for Young Scientist (Grant No. 51905105), and the Natural Science Foundation of Guangdong Province—Regular Project.

The data set used in this work was obtained from the National Key Basic Research Program of China (973 Program) (Grant No. 2015CB058103).

Appendix
The parameters of the optimal parameter identification result

- Cutterhead torque
- Pushing pressure
- Cutterhead thrust
- Stroke detection of the left gripper cylinder
- Stroke detection of the right gripper cylinder
- Pressure of the propulsion pump
- Cutterhead power
- Pressure of the right gripper small cavity
- Displacement of the right torque cylinder
- Displacement of the left torque cylinder
- Torque of motor 6
- Torque of motor 5
- Torque of motor 4
- Extension pressure of the left torque cylinder
- Torque of motor 7
- Torque of motor 2
- Extension pressure of the right torque cylinder
- Torque of motor 3
- Recovery pressure of the left torque cylinder
- Power of motor 5
- Torque of motor 8
- Stroke detection of the left propulsion cylinder
- Pressure of the left gripper small cavity
- Displacement of the right shield
- Torque of motor 1
- Power of motor 4
- Torque of motor 9
- Power of motor 1
- Power of motor 2
- Propulsion displacement
- Stroke detection of the right propulsion cylinder
- Power of motor 2
- Pressure of the left dragging cylinder
- Temperature of inverter 2
- Displacement of the left shield
- Power of motor 6
- Recovery pressure of the right torque cylinder
- Pressure of the right dragging cylinder
- Torque of motor 10

- Brake pressure of the cutterhead
- Pressure of the gripper
- Pressure of the right wedge cylinder
- Temperature of the hot-water tank
- Power of motor 7
- Temperature of the internal circulating water tank
- Pressure of the top shield
- Temperature of the cold-water tank
- Power of motor 8
- Pressure of the left wedge cylinder
- Power of motor 9
- Pressure of the left shield
- Pressure of the gripper pump
- Temperature of the main cooler inlet water
- Current of motor 5
- Power of motor 10
- Temperature of reducer 1
- Pressurized pressure of the main drive
- Temperature of inverter 1
- Flow of the outer seal cavity
- Current of motor 3
- Current of motor 4
- Temperature of reducer 4
- Given speed of the cutterhead
- Lubrication pressure of pump 1
- Current of motor 1
- Current of motor 2
- Given value of the cutterhead speed potentiometer
- Cutterhead speed display value
- Given frequency
- Current of motor 6
- Gear oil temperature
- Current of motor 8
- Current of motor 10
- Support pressure on left
- Lubrication pressure of pump 4
- Current of motor 7
- Given value of the propulsion speed potentiometer
- Given propulsion speed percentage
- Pressure gear return pump outlet
- Current of motor 9

REFERENCES

[1] Q. Liu, X. Huang, Q. Gong, L. Du, Y. Pan, and J. Liu, "Application and development of hard rock tbm and its prospect in china," *Tunnelling and Underground Space Technology*, vol. 57, pp. 33–46, 2016.

[2] Q. Gong and J. Zhao, "Development of a rock mass characteristics model for tbm penetration rate prediction," *International Journal of Rock Mechanics and Mining Sciences*, vol. 46, no. 1, pp. 8–18, 2009.

[3] U. Ates, N. Bilgin, and H. Copur, "Estimating torque, thrust and other design parameters of different type tbms with some criticism to tbms used in turkish tunneling projects," *Tunnelling and Underground Space Technology*, vol. 40, pp. 46–63, 2014.

[4] R. Mikaeil, M. Z. Naghadehi, and F. Sereshki, "Multifactorial fuzzy approach to the penetrability classification of tbm in hard rock conditions," *Tunnelling and Underground Space Technology*, vol. 24, no. 5, pp. 500–505, 2009.

[5] S. Yagiz, "New equations for predicting the field penetration index of tunnel boring machines in fractured rock mass," *Arabian Journal of Geosciences*, vol. 10, no. 2, p. 33, 2017.

[6] R. Gertsch, L. Gertsch, and J. Rostami, "Disc cutting tests in colorado red granite: Implications for tbm performance prediction," *International Journal of Rock Mechanics and Mining Sciences*, vol. 44, no. 2, pp. 238–246, 2007.

[7] J. Xue, Y. Xia, Z. Ji, and X. Zhou, "Soft rock cutting mechanics model of tbm cutter and experimental research," in *International Conference on Intelligent Robotics and Applications*. Springer, 2009, pp. 383–391.

[8] M. Entacher, S. Lorenz, and R. Galler, "Tunnel boring machine performance prediction with scaled rock cutting tests," *International Journal of Rock Mechanics and Mining Sciences*, vol. 70, pp. 450–459, 2014.

[9] T. Kasper and G. Meschke, "On the influence of face pressure, grouting pressure and tbm design in soft ground tunnelling," *Tunnelling and Underground Space Technology*, vol. 21, no. 2, pp. 160–171, 2006.

[10] C. Su, Y. Wang, H. Zhao, P. Su, C. Qu, Y. Kang, T. Huang, Z. Cai, and L. Wang, "Analysis of mechanical properties of two typical kinds of cutterheads of shield machine," *Advanced Science Letters*, vol. 4, no. 6-7, pp. 2049–2053, 2011.

[11] H. Tao, W. Jingcheng, and Z. Langwen, "Prediction of hard rock tbm penetration rate using random forests," in *The 27th Chinese Control and Decision Conference (2015 CCDC)*. IEEE, 2015, pp. 3716–3720.

[12] W. Sun, M. Shi, C. Zhang, J. Zhao, and X. Song, "Dynamic load prediction of tunnel boring machine (tbm) based on heterogeneous in-situ data," *Automation in Construction*, vol. 92, pp. 23–34, 2018.

[13] S. Mahdevari, K. Shahriar, S. Yagiz, and M. A. Shirazi, "A support vector regression model for predicting tunnel boring machine penetration rates," *International Journal of Rock Mechanics and Mining Sciences*, vol. 72, pp. 214–229, 2014.

[14] F. Ling, W. Jingcheng, G. Yang, L. Chuang, and Z. Langwen, "Prediction of tbm penetration rate based on the model of pls-fnn," in *2013 25th Chinese Control and Decision Conference (CCDC)*. IEEE, 2013, pp. 1295–1299.

[15] X. Gao, M. Shi, X. Song, C. Zhang, and H. Zhang, "Recurrent neural networks for real-time prediction of tbm operating parameters," *Automation in Construction*, vol. 98, pp. 225–235, 2019.

[16] S. Hochreiter and J. Schmidhuber, "Long short-term memory," *Neural Computation*, vol. 9, no. 8, pp. 1735–1780, 1997.